Revisiting Snoke's (1987) Spectral Expressions: Coefficient Correction and Its Implications for Dynamic Insights

Minkyung Son

Earthquake Research Center, Korea Institute of Geoscience and Mineral Resources
kersti@kigam.re.kr
ORCID: 0000-0003-4862-8510

Revisiting Snoke's (1987) Spectral Expressions: Coefficient Correction and Its Implications for Dynamic Insights

Minkyung Son[1*]

[1]Earthquake Research Center, Korea Institute of Geoscience and Mineral Resources, 124 Gwahak-ro, Yuseong-gu, Daejeon, 34132, Republic of Korea

[*]Corresponding author: Minkyung Son (kersti@kigam.re.kr)

KEY POINTS

- Snoke's low-frequency spectral-level coefficient is 2, not $4^{1/4}$.
- This $\sqrt{2}$ error underestimates seismic moment by $\sqrt{2}$ and M_w by ~0.1.
- Stress drop, radiated energy, apparent stress, and energy budgets change accordingly.

ABSTRACT

Source parameters such as seismic moment, corner frequency, stress drop, radiated energy, and apparent stress are often derived from the Brune (1970) source spectrum. Building on this, Andrews (1986) formulated analytical relations that link those parameters to spectral integrals of squared velocity and displacement, and Snoke (1987) introduced an approximation that enables their practical estimation from limited-band data. However, subsequent studies have adopted inconsistent numerical coefficients in Snoke's expression for the low-frequency spectral level. Our rederivation confirms that the correct coefficient is 2, rather than $4^{1/4}$, and shows that the discrepancy arises from a computational oversight in the original formulation. We further clarify how Snoke's integral approximation extends to radiated energy and apparent stress, highlighting the linkage between inferred source parameters, dynamic rupture process, and energy balance. This re-examination would support consistent use of spectral formulations in earthquake source parameter estimation and underscore the need for caution when estimating and interpreting source parameters, especially secondary quantities.

INTRODUCTION

Earthquake source parameters provide critical insights into faulting and energy radiation processes. Their estimation often relies on spectral modeling, particularly in quantifying seismic moment, corner frequency, stress drop, radiated energy, and apparent stress. A widely used spectral model that embodies these characteristics is the Brune (1970; 1971) model, which describes the far-field source spectrum with two asymptotic behaviors: a constant plateau at low frequencies and an f^{-2} decay at high frequencies.

Building on the asymptotic characteristics of the Brune model, Snoke (1987) proposed a method for estimating source parameters by approximating the displacement spectrum across specific frequency ranges. His approach incorporates squared spectral integrals of squared velocity and displacement, denoted of J and K, which were originally formulated in analytical form by Andrews (1986). This approximation enables stable evaluation of the integrals and relates observable spectral quantities to key source parameters. As a result, Snoke's method has been widely used and has formed the basis for many subsequent studies (Gibowicz et al., 1991; Kwiatek and Ben-Zion, 2016; Chen et al., 2025).

However, later studies differ in how they implement Snoke's low-frequency spectral level expression, specifically Equation (10) in Snoke (1987). Some retain the original coefficient of $4^{1/4}$ (Garcia-Garcia et al., 1996; Kumar et al., 2005; Rhee and Sheen, 2016; Raub et al., 2017; Lim et al., 2024), whereas others adopt the value 2, often citing Andrews (1986) alongside Snoke (Urbancic et al., 1996; Kwiatek et al., 2010; Ahn et al., 2025). This discrepancy, which corresponds to a factor of $2/4^{1/4}$ (i.e., $\sqrt{2}$), leads to a systematic 1.4-fold difference in seismic moment estimates and an 0.1-unit shift in moment magnitude.

In this study, we revisit Snoke's (1987) integral formulation by analytically re-examining its derivation from the Brune source model and show that the coefficient in his Equation (10) should be corrected from $4^{1/4}$ to 2. We also clarify how Snoke's approximation for the squared spectral integrals extends to limited-band data, as noting that the squared velocity integral represents energy flux in the far field. This links earthquake source parameters to strain-rate evolution and energy radiation, and serves as a reminder of underlying assumptions and uncertainties in such estimates.

ANALYTICAL DERIVATION AND COEFFICIENT CORRECTION

Source Spectra and Definition of J and K

The Brune (1970; 1971) source model is one of the most widely used for characterizing earthquake source spectra. It describes the far-field displacement amplitude in the frequency domain as

$$|U(f)| = \frac{\Omega_0}{1+\left(\frac{f}{f_c}\right)^2}, \tag{1}$$

where Ω_0 is the low-frequency level, proportional to the seismic moment M_0, and f_c is the corner frequency. At low frequencies ($f \ll f_c$), the displacement spectrum approaches a constant value (Ω_0), whereas at high frequencies ($f \gg f_c$), the spectrum decays as f^{-2} (Figure 1).

Building on this spectral form, early studies (Andrews, 1986; Snoke, 1987) linked spectral observations to earthquake source parameters by defining two key squared spectral integrals, J and K. The squared velocity integral J, which uses the relation $|V(f)| = |2\pi f U(f)|$, is given by:

$$J = 2\int_0^\infty |V(f)|^2\, df = 2\int_0^\infty |2\pi f U(f)|^2\, df = 2\int_0^\infty |\omega U(\omega)|^2\, df, \tag{2}$$

and the squared displacement integral K is defined as

$$K = 2\int_0^{\infty}|U(f)|^2 \, df = 2\int_0^{\infty}|U(\omega)|^2 \, df. \tag{3}$$

Here, the first forms of J and K correspond to the definitions of S_{V2} and S_{D2} in Andrews (1986), whereas the last forms follow the notation adopted by Snoke (1987). Although their forms differ, the integral values are identical under the transformation $\omega = 2\pi f$ because the Brune spectrum depends only on the ratio f/f_c (or ω/ω_c), so Snoke's ω-based notation represents the same spectral shape and is still evaluated over f.

Analytical Derivation of J and K

We now derive explicit expressions for the squared spectral integrals J and K, expressed in terms of the low-frequency spectral level Ω_0 and the corner frequency f_c. Substituting $U(f)$ into the definition of J from Equation (2) and introducing the change of variables $x = f/f_c$ (with $df = f_c \, dx$), we obtain

$$J = 2(2\pi)^2\Omega_0^2 f_c^3 \int_0^{\infty}\frac{x^2 \, dx}{(1+x^2)^2}. \tag{4}$$

Using the standard result $\int_0^{\infty} x^2/(1+x^2)^2 \, dx = \pi/4$, this yields

$$J = 2\pi^3\Omega_0^2 f_c^3 = \frac{1}{4}\Omega_0^2(2\pi f_c)^3. \tag{5}$$

Likewise, the squared displacement integral K can be obtained from Equation (3) as

$$K = 2\Omega_0^2 f_c \int_0^{\infty}\frac{dx}{(1+x^2)^2} = 2\Omega_0^2 f_c \frac{\pi}{4} = \frac{1}{4}\Omega_0^2(2\pi f_c). \tag{6}$$

Equations (5) and (6) are consistent with the formulation of Andrews (1986). These relations can be algebraically inverted to solve for Ω_0 and f_c in terms of J and K. This forms the basis for estimating source parameters from spectral data, an approach later adopted by Snoke (1987) but with a coefficient error that we address in the following section.

Low-Frequency Level Coefficient Correction

We solve for the corner frequency f_c and the low-frequency spectral level Ω_0 using the analytic expressions for J and K. From Equations (5) and (6), dividing J by K eliminates Ω_0 and yields $J/K = 4\pi^2 f_c^2$, which leads to the expression for the corner frequency

$$f_c = \left(\frac{J}{4\pi^2 K}\right)^{1/2} = \frac{1}{2\pi}\sqrt{\frac{J}{K}}. \tag{7}$$

This form is identical to Equation (10) in Andrews (1986) and Equation (11) in Snoke (1987). Substituting Equation (7) into Equation (6) to solve for Ω_0 gives

$$K = \frac{\pi}{2}\Omega_0^2 \frac{1}{2\pi}\sqrt{\frac{J}{K}}. \tag{8}$$

Rearranging yields

$$\Omega_0^2 = \frac{K}{\frac{1}{4}\left(\frac{J}{K}\right)^{1/2}} = 4\frac{K^{3/2}}{J^{1/2}} = 4\sqrt{\frac{K^3}{J}}, \tag{9}$$

and taking the square root gives

$$\Omega_0 = 2\left(\frac{K^3}{J}\right)^{1/4}. \tag{10}$$

Equation (10) shows that the coefficient in front of $(K^3/J)^{1/4}$ is 2, which is consistent with the expression by Andrews (1986) but differs from the $4^{1/4}$ used in Equation (10) of Snoke (1987). Because this result follows directly from Snoke's own definition, the coefficient $4^{1/4}$ in his formulation should be replaced by 2. This is supported by two internal consistency checks. First, Snoke's Equations (7) and (9) both express Brune's stress drop in terms of J and K; equating them and solving for Ω_0 yields the same form as Equation (10) here. Second, substituting Snoke's Equation (10) into his Equation (6) does not reproduce his Equation (11), whereas the equivalence is recovered only when coefficient is 2.

EFFECTS AND IMPLICATIONS OF COEFFCIENT CORRECTION

Seismic Moment and Stress Drop

The change of the coefficient from $4^{1/4}$ to 2 leads to an underestimation of M_0 by a factor of $\sqrt{2}$, corresponding to ~0.1 unit in moment magnitude. This difference propagates into stress drop. Brune (1970; 1971) linked M_0 to f_c based on the assumption of 100 % stress drop occurring instantaneously over a circular fault of radius r (i.e., infinite rupture velocity) and the S-to-P wave conversion factor as 0.8. Then, the static stress drop $\Delta\sigma_B$ can be expressed as

$$\Delta\sigma_B = h\gamma\Omega_0 f_c^3 = hM_0 f_c^3 = \frac{7}{16}\frac{M_0}{r^3}, \tag{11}$$

where $h = \frac{7}{16}\left(\frac{2\pi}{\sqrt{7\pi/4}}\frac{1}{\beta}\right)^3$, $\gamma = \frac{4\pi\rho\beta^3}{R_S}$, and $r = \frac{k\beta}{f_c}$ with $k = \frac{\sqrt{7\pi/4}}{2\pi} = \frac{2.34}{2\pi} = 0.372$. β is the S-wave velocity; if the medium is depth-dependent (i.e., 1-D velocity model), β^3 may be approximated as $\beta_s^{2.5}\beta_r^{0.5}$, where subscripts s and r denote the source and receiver regions, respectively (e.g., Aki and Richards, 2002). ρ is the density, and $R_S = \sqrt{2/5}$ is the spherical average of the double-couple S-wave radiation pattern.

From Equation (11), underestimating M_0 by a factor of $\sqrt{2}$ due to the coefficient error leads to a proportional underestimation of $\Delta\sigma_B$ by the same factor when f_c is determined independently, for example by spectral curve fitting. If f_c is instead obtained using Snoke's formulation, $\Delta\sigma_B$ increases by $\sqrt{2}$, because Snoke rewrote f_c in terms of Ω_0 and J using Equation (5):

$$f_c = \frac{1}{\pi}\left(\frac{J}{2\Omega_0^2}\right)^{1/3}. \tag{12}$$

Equation (11) shows that stress drop scales with f_c^3. Stress drop estimates are therefore inherently sensitive to how f_c is determined and often show large scatter (e.g., Abercrombie, 2021; Son and Chaves, 2025). Snoke's formulation for f_c in Equation (12) instead makes $\Delta\sigma_B$ linear in J/Ω_0^2. In the ideal broadband limit, J is a model-independent observable (e.g., Ji et al., 2022).

In practice, however, J is estimated from band-limited data and thus involves extrapolation beyond the available bandwidth (Di Bona and Rovelli, 1988; Ide and Beroza, 2001). Snoke (1987) implicitly assumed a Brune-type spectrum with f_c lying between f_1 and f_2, a constant level Ω_0 below f_1 and an f^{-2} decay above f_2 (Figure 1). This yields a band-limited estimate J_{Snoke}, constructed from observable spectral values over $f \in (f_1, f_2)$ (see also Appendix):

$$J_{Snoke} = \frac{2}{3}[\omega_1\Omega_0]^2 f_1 + 2\int_{f_1}^{f_2} |\omega U(\omega)|^2 df + 2|\omega_2 U(\omega_2)|^2 f_2. \tag{13}$$

This extrapolation approach has been widely adopted in subsequent studies to estimate far-field radiated energy from band-limited observations (Mayeda and Walter, 1996; Collins and Yong, 2000; Baltay et al., 2014; Bindi et al., 2025).

Radiated Energy and Apparent Stress

The radiated energy can be defined as the traction-velocity flux integrated over a radiating boundary (i.e., a closed far-field surface S_0), as given by the first form of Equation (14) (e.g., Rivera and Kanamori, 2005). Under the far-field approximation, this definition reduces to an expression in terms of the particle velocity. Applying Parseval's theorem then yields a spectral form involving the squared velocity spectrum (e.g., Vassiliou and Kanamori, 1982; Andrews, 1986). For S-waves:

$$E_R = \int_{S_0} \int (\boldsymbol{\sigma}_{\boldsymbol{m}} \cdot \mathbf{v}) \cdot \mathbf{n} \ dtdS = 4\pi\rho\beta \int_{-\infty}^{\infty} |\mathbf{v}(t)|^2 dt = 8\pi\rho\beta \int_0^{\infty} |\tilde{\mathbf{v}}(f)|^2 \ df \qquad (14)$$

Here, $\boldsymbol{\sigma}_m$ denotes the stress tensor associated with the radiated field, representing only the portion of stress that contributes to seismic wave radiation. $\mathbf{v}(t)$ is the particle velocity vector on S_0, $\mathbf{n}$ is the outward unit normal, and $\tilde{\mathbf{v}}(f)$ denotes the Fourier transform of $\mathbf{v}(t)$. The last expression involves the squared integral of the velocity spectrum and is therefore equivalent to $4\pi\rho\beta J$.

Normalizing the radiated energy E_R by the seismic moment M_0 gives the apparent stress (Wyss and Brune, 1971; McGarr, 1999) as

$$\sigma_a = \mu \frac{E_R}{M_0} = \frac{E_R}{DA} = \frac{\sigma_0 + \sigma_1}{2} - \bar{\sigma}_f. \qquad (15)$$

Here, μ is the shear modulus, D is the averaged total slip over the fault plane, and A is rupture area. The loading (driving) shear stress in the surrounding rock decreases from σ_0 to σ_1 along a linear elastic unloading path of the loading system governed by the system stiffness, and $\bar{\sigma}_f$ represents an average of the resisting stress σ_f on the fault plane during the slip D (Figure 2).

Note that the definitions of E_R and σ_a are independent of any particular source spectral model. However, in practice, estimating E_R requires model assumption since available observations are band-limited. For example, if E_R is obtained by directly integrating the squared velocity spectrum based on Snoke's extrapolation approach (i.e., by using J_{Snoke}), the underestimation of M_0 caused by Snoke's coefficient error linearly increases σ_a by $\sqrt{2}$, following the first expression in the following equation:

$$\sigma_a = \mu \frac{4\pi\rho\beta J}{M_0} = 4\pi\rho^2\beta^3 \frac{2\pi^3\Omega_0^2 f_c^3}{M_0} \frac{\gamma^2}{\gamma^2} = \frac{1}{5}\pi^2 M_0 f_c^3 / \beta^3. \quad (16)$$

If, instead, E_R is evaluated using the analytic solution for J in Equation (5) (i.e., by adopting modeled spectra over the full frequency range), an underestimation of M_0 decreases σ_a by $\sqrt{2}$, following the last expression in Equation (16). Some studies (Rhee and Sheen, 2016; Lim et al., 2024; Ahn et al., 2025) further implement an iterative approach in which Ω_0 is reintroduced into J_{Snoke}. This makes the coefficient error propagate nonlinearly, although the nonlinear effect is usually small because the dependence on Ω_0 is cubically scaled by the low-frequency limit f_1 (Equation 13).

From Static Parameters to Dynamic Insights

Correcting the low-frequency spectral coefficient alters the estimates of key source parameters such as M_0, $\Delta\sigma$, E_R, and σ_a. These quantities reflect the time-integrated effects of dynamic rupture and are linked through energy balance. The total potential energy released can be written as Equation (17), separating the radiated energy E_R and the dissipative terms E_G (fracture energy) and E_F (frictional energy) (e.g., Rivera and Kanamori, 2005; Lambert and Lapusta, 2023; Krammer et al., 2024):

$$\Delta W = \int_V \int \boldsymbol{\sigma}:\dot{\boldsymbol{\varepsilon}}\, dt\, dV = \int_V \int \sigma_{ij} d\varepsilon_{ij}\, dV = \int_A \frac{\sigma_0+\sigma_1}{2} D\, dA = E_R + E_G + E_F. \quad (17)$$

Here, $\boldsymbol{\sigma}:\dot{\boldsymbol{\varepsilon}} = \sigma_{ij}\dot{\varepsilon}_{ij}$ denotes the stress-strain rate power density within the volume V inside S_0. The volume integral reduces to work on the fault plane of area A, where the slip D represents the average final displacement produced during the linear elastic unloading of the loading stress from σ_0 to σ_1 (Figure 2). E_G includes all dissipative processes associated only with crack growth localized near the crack tip or within the cohesive zone, and E_G/A corresponds to the breakdown work (density) W_b in cohesive-zone models. The remaining dissipative part, E_F, accounts for frictional or other non-localized processes, including heat generation along the slipping fault, and represents late-time dissipation that dominates the tail of the energy budget. This form of the energy balance remains unchanged even when gravitational or rotational kinetic contributions are considered.

Thus, as shown in Figure 2a, the static stress drop $\Delta\sigma = \sigma_0 - \sigma_1$ and the apparent stress σ_a together constrain the partitioning of released energy between seismic radiation and fracture processes when the final stress equals the minimum resisting stress during slip, $\sigma_1 = \sigma_f^{min}$. This condition, corresponding to the absence of undershoot or overshoot, simplifies Equation (18) to Equation (19):

$$\Delta W - E_F = E_R + E_G = \sigma_a DA + GA = \frac{\Delta\sigma}{2} DA + \left(\sigma_1 - \sigma_f^{min}\right) DA, \quad (18)$$

$$E_R + E_G = \sigma_a DA + GA = \frac{\Delta\sigma}{2} DA. \quad (19)$$

In Equation (19), the static stress drop $\Delta\sigma$ represents the total stress release that accounts for both seismic radiation and the localized breakdown work near the rupture front, whereas the apparent stress σ_a quantifies the portion of this release that is converted into seismic radiation and observed in ground motions.

Because correcting the low-frequency coefficient changes both $\Delta\sigma$ and σ_a, it alters their ratio and therefore affects the fracture energy inferred under the assumption $\sigma_1 = \sigma_f^{min}$. Under this assumption, the energy-based radiation efficiency η_r^E in Equation (20) reduces to the radiation efficiency or ratio η_r in Equation (21) (e.g., Venkataraman and Kanamori, 2004), and the inferred fracture energy density G' follows as in Equation (22) (e.g., Abercrombie and Rice, 2005):

$$\eta_r^E = \frac{E_R}{E_R + E_G}, \tag{20}$$

$$\eta_r = \frac{\sigma_a}{\Delta\sigma/2}, \tag{21}$$

$$G' = \left(\frac{\Delta\sigma}{2} - \sigma_a\right) D = \frac{\Delta\sigma}{2}(1 - \eta_r) D. \tag{22}$$

Accordingly, if $\Delta\sigma$ is underestimated while σ_a is overestimated, both by a factor of $\sqrt{2}$ as implied by Equations (11) and (15), η_r becomes twice its true value, leading to a corresponding decrease in the inferred fracture energy density G'.

More generally, the impact of such misestimations can be explored using the ratio $\hat{G}'/G'$ in Figure 3, where the hat denotes misestimated quantities. The curves show that $\hat{G}'/G'$ decreases rapidly as η_r increases. In this bias case, the inferred fracture energy may be underestimated by more than an order of magnitude for high efficiency events, and the bias becomes stronger under undershoot conditions (see also Figures 2b and 2c). This view is likely to be more relevant for small earthquakes, where undershoot effects can become significant in the energy balance (Gabriel et al., 2024), since Snoke-based spectral analyses have been widely applied in that magnitude range.

CONCLUSION

This study revisits Snoke's (1987) spectral integral formulation and corrects the low-frequency coefficient from $4^{1/4}$ to 2, which corresponds to 1.4-fold reduction in seismic moment estimates and an 0.1-unit decrease in moment magnitude. The corrected coefficient thereby refines the quantitative link between earthquake source parameters and their dynamic implications, emphasizing the sensitivity of inferred energy balance to even small inconsistencies. Such sensitivity can introduce systematic bias in derived quantities, particularly in secondary parameters such as apparent stress, stress drop, and fracture energy. Recognizing these effects is essential for exploring how earthquakes generate and dissipate energy.

DATA AND RESOURCES

All data used in this paper came from published sources listed in the references.

DECLARATION OF COMPETING INTERESTS

The authors declare no competing interests.

ACKNOWLEDGEMENTS

The author acknowledges B. S. Ahn and S. Lee. This study was supported by the Basic Research Project of KIGAM funded by the Ministry of Science and ICT (MSIT, Republic of Korea).

FULL MAILING ADDRESS

Minkyung Son (kersti@kigam.re.kr)

Earthquake Research Center, Korea Institute of Geoscience and Mineral Resources, 124 Gwahak-ro, Yuseong-gu, Daejeon, 34132, Republic of Korea

REFERENCES

Abercrombie, R. E. (2021). Resolution and uncertainties in estimates of earthquake stress drop and energy release, Phil. Trans. R. Soc. A. 379, no. 2196, 20200131. doi: 10.1098/rsta.2020.0131

Abercrombie, R. E. and Rice, J. R. (2005). Can observations of earthquake scaling constrain slip weakening? Geophys. J. Int. 162, no. 2, 406-424. doi: 10.1111/j.1365-246X.2005.02579.x

Ahn, B. S., Kang, T.-S., and Yoo, H. J. (2025). Source parameter estimation using site-corrected source spectra for the 2019 Ridgecrest earthquake sequence in Southern California, Bull. Seismol. Soc. Am. 115, no.3, 927-946. doi: 10.1785/0120240157

Aki, K., and G. P. Richards (2002). Quantitative Seismology, University Science Books, Sausalito, California, 441 pp.

Andrews, D. J. (1986). Objective determination of source parameters and similarity of earthquakes of different size, in Earthquake Source Mechanics, S. Das, J. Boatwright, and C. H. Scholz (Editors), Geophysical Monograph Series, Vol. 37, American Geophysics Union, Washington, D. C., 259-267. doi: 10.1029/GM037p0259

Baltay, A. S., Beroza, G. C., and Ide, S. (2014). Radiated energy of great earthquakes from teleseismic empirical Green’s function, Pure Appl. Geophys. 171, 2841-2862. doi: 10.1007/s00024-014-0804-0

Bindi, D., Oth, A., Parolai, S., Picozzi, M., and Spallarossa, D. (2025). Interevent variability in ground-motion prediction models: The role of the source parameter selection, Bull. Seismol. Soc. Am. 115, no. 6, 2857-2866. doi: 10.1785/0120250098

Brune, J. N. (1970). Tectonic stress and the spectra of seismic shear waves from earthquakes, J. Geophys. Res. 75, no. 26, 4997-5009. doi: 10.1029/JB075i026p04997

Brune, J. N. (1971). Correction [to “Tectonic stress and the spectra, of seismic shear waves from earthquakes”], J. Geophys. Res. 76, no 20, 4711-5002. doi: 10.1029/JB076i020p05002

Chen, X., Kwiatek, G., Bindi, D., Becker, D., Bohnhoff, M., Cotton, F., and Martinez-Garzon, P. (2025). Stress drop variations of (a)seismic fatul segments in the Sea of Marmara region (Northwestern Turkiye) supported by different methodological approaches, Bull. Seismol. Soc. Am. 115, no. 3, 1016-1030. doi: doi.org/10.1785/0120240128

Cocco, M., Aretusini, S., Cornelio, C., Nielsen, S. B., Spagnuolo, E., Tinit, E., and Di Toro, G. (2023). Fracutre energy and breakdown work during earthquakes, Annu. Rev. Earth Planet. Sci. 51, 217-252. doi: 10.1146/annurev-earth-071822-100304

Collins, D. S. and Yong, R. P. (2000). Lithological contorls on seismicity in granitic rocks, Bull. Seismol. Soc. Am. 90, no. 3, 709-723. doi: 10.1785/0119990142

Di Bona, M. and Rovelli, A. (1988). Effects of the bandwidth limitation on stress drops estimated from integrals of the ground motion, Bull. Seismol. Soc. Am. 78, no. 5, 1818-1825. doi: 10.1785/BSSA0780051818

Gabriel, A.-A., Garagash, D. I., Palgunadi, K. H., and Mai, P. M. (2024). Fault size-dependent fracture energy explains multiscale seismicity and cascading earthquakes, Science 385, no. 6707, eadj9587. doi: 10.1126/science.adj9587

Garcia-Garcia, J. M., Vidal, F., Romacho, M. D., Martin-Marfil, J. M., Psadas, A., and Luzon, F. (1996). Seismic source parameters for microearthquakes of the Granada basin (southern Spain), Tectonophysics 261, no. 1-3, 51-66. doi: 10.1016/0040-1951(96)00056-X

Gibowicz, S. J., Young, R. P., Talebi, S, and Rawlence, D. J. (1991). Source parameters of seismic events at the underground research laboratory in Mantoba, Canada: Scaling relations for events with moment magnitude smaller than -2, Bull. Seismol. Soc. Am. 81, no. 4, 1157-1182. doi: 10.1785/BSSA0810041157

Ide, S. and Beroza, G. C. (2001). Does apparent stress vary with earthquake size? Geophys. Res. Lett. 28, no. 17, 3349-3352. doi: 10.1029/2001GL013106

Ji, C., Archuleta, R. J., and Wang, Y. (2022). Variability of spectral estimates of stress drop reconciled by radiated Energy. Bull. Seismol. Soc. Am. 112, no. 4, 1871-1885. doi: 10.1785/0120210321

Krammer, D. S., McLaskey, G. C., Abercrombie, R. E., Ampuero, J.-P., Cattania, C., Cocco, M., Zilio, L. D., Dresen, G., Gabriel, A.-A., Ke, C.-Y., Marone, C., Selvadurai, P. A., and Tinti, E. (2024). Earthquake energy dissipation in a fracture mechanics framework, Nat. Commun. 15, 4736. doi: 10.1038/s41467-024-47970-6

Kumar, D., Sarkar, I., Sriram, V., and Khattri, K. N. (2005). Estimation of the source parameters of the Himalaya earthquake of October 19, 1991, average effective shear wave attenuation parameter and local site effects from accelerograms, Tectonophysics 47, no. 1-2, 1-24. doi: 10.1016/j.tecto.2005.06.006

Kwiatek, G. and Ben-Zion, Y. (2016). Theoretical limits on detection and analysis of small earthquakes, J. Geophys. Res. 121, no. 8, 5898-5916. doi: 10.1002/2016JB012908

Kwiatek, G., Plenkers, K., Nakatani, M., Yabe, Y., Dresen, G., and JAGUARS-Group (2010). Frequency-magnitude characteristics down to magnitude -4.4 for induced seismicity recorded at Mponeng Gold Mine, South Africa, Bull. Seismol. Soc. Am. 100, no. 3, 1165-1173. doi: 10.1785/0120090277

Lambert, V. and Lapusta, N. (2023). Absolute stress levels in models of low-heat faults: Links to geophysical observables and differences for crack-like ruptures and self-healing pulses, Earth Planet. Sci. Lett. 618, 118277. doi: 10.1016/j.epsl.2023.118277

Lim, H., C. S. Cho, and M. Son (2024). The 2022 Goesan earthquake of the moment magnitude 3.8 along the buried fault in the central Korean Peninsula, J. Seismol. 28, 519-534, doi: 10.1007/s10950-024-10201-y

Mayeda, K. and W. R. Walter (1996). Moment, energy, stress drop, and source spectra of western United States earthquakes from regional coda envelopes, J. Geophys. Res. 101, no. B5, 11195-11208. doi: 10.1029/96JB00112

McGarr, A. (1999). On relating apparent stress to the stress causing earthquake fault slip, J. Geophys. Res. 104, no. B2, 3003-3011. doi: 10.1029/1998JB900083

Raub, C., Martinez-Garzon, P., Kwiatek, G., Bohnhoff, M., and Dresen, G. (2017). Variations of seismic b-value at different stages of the seismic cycle along the North Anatolian Fault

Zone in northwestern Turkey, Tetonophysics 712-713, 232-248. doi: 10.1016/j.tecto.2017.05.028

Rhee, H.-M. and Sheen, D.-H. (2016). Lateral variation in source parameters of earthquakes in the Korean Peninsula, Bull. Seismol. Soc. Am. 106, no. 5, 2266-227. doi: 10.1785/0120160085

Rivera, L. and Kanamori, H. (2005). Representations of the radiated energy in earthquakes, Geophys. J. Int 162, no. 1, 148-155. doi: doi: 10.1111/j.1365-246X.2005.02648.x

Snoke, J. A. (1987). Stable determination of (Brune) stress drops, Bull. Seismol. Soc. Am. 77, no. 2, 530–538. doi: 10.1785/BSSA0770020530

Son, M. and Chaves, E. J. (2025). Investigating Corner-Frequency Uncertainties: Insights from Six Earthquakes (Mw 3.2–3.8) in Ridgecrest, California, and the Korean Peninsula, Bull. Seismol. Soc. Am. 115, no. 3, 1189-1211. doi: 10.1785/0120240149

Ulbancic, T. I., Trifu, C.-I., Mercer, R. A., Feustel, A. J., and Alexander, J. A. G. (1996). Automatic time-domain calculation of source parameters for the analsyis of induced seismicity, Bull. Seismol. Soc. Am. 86, no. 5, 1627-1633. doi: 10.1785/BSSA0860051627

Vassiliou, M. S. and Kanamori, H. (1982). The energy release in earthquakes, Bull. Seismol. Soc. Am. 72, no. 2, 371-387. doi: 10.1785/BSSA0720020371

Venkataraman, A. and Kanamori, H. (2004). Effect of directivity on estimates of radiated seismic energy, J. Geophys. Res. 109, B04301. doi: 10.1029/2003JB002548

Wyss, M. and Brune, J. N. (1971). Regional variations of source properties in Southern California estimated from the ratio of short- to long-period amplirudes, Bull. Seismol. Soc. Am. 61, no. 5, 1153-1167. doi: 10.1785/BSSA0610051153

FIGURES

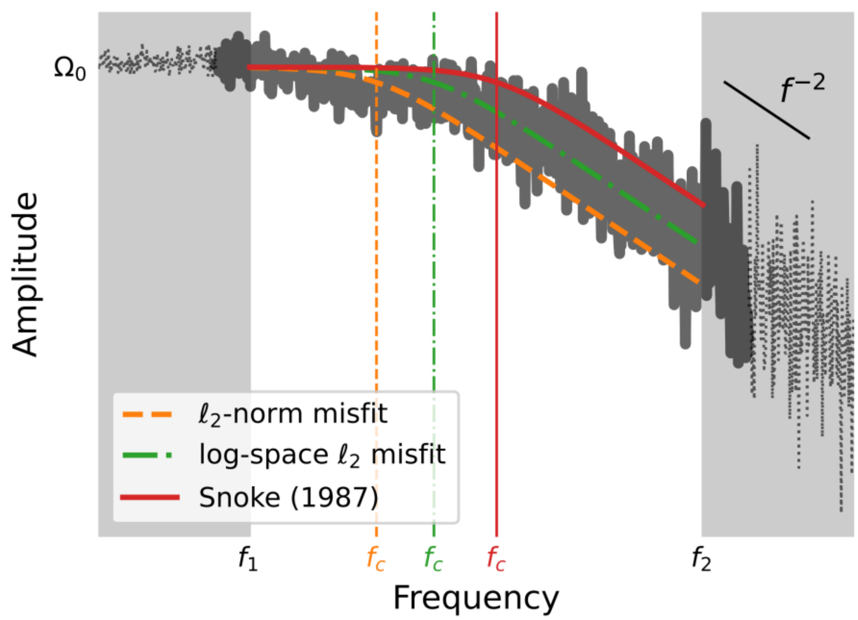

Figure 1. Brune (1970) source spectra in log-log axes (dashed, dash-dotted, and solid lines): low-frequency spectral level (long-period plateau) Ω_0, corner frequency f_c, and high-frequency f^{-2} decay. Gray shaded regions denote off-band frequencies outside the usable bandwidth $[f_1, f_2]$. The background curve represents an example spectrum, with the solid segment lying within the observable band (which may extend beyond $[f_1, f_2]$) and the dotted segments lying outside the observable band.

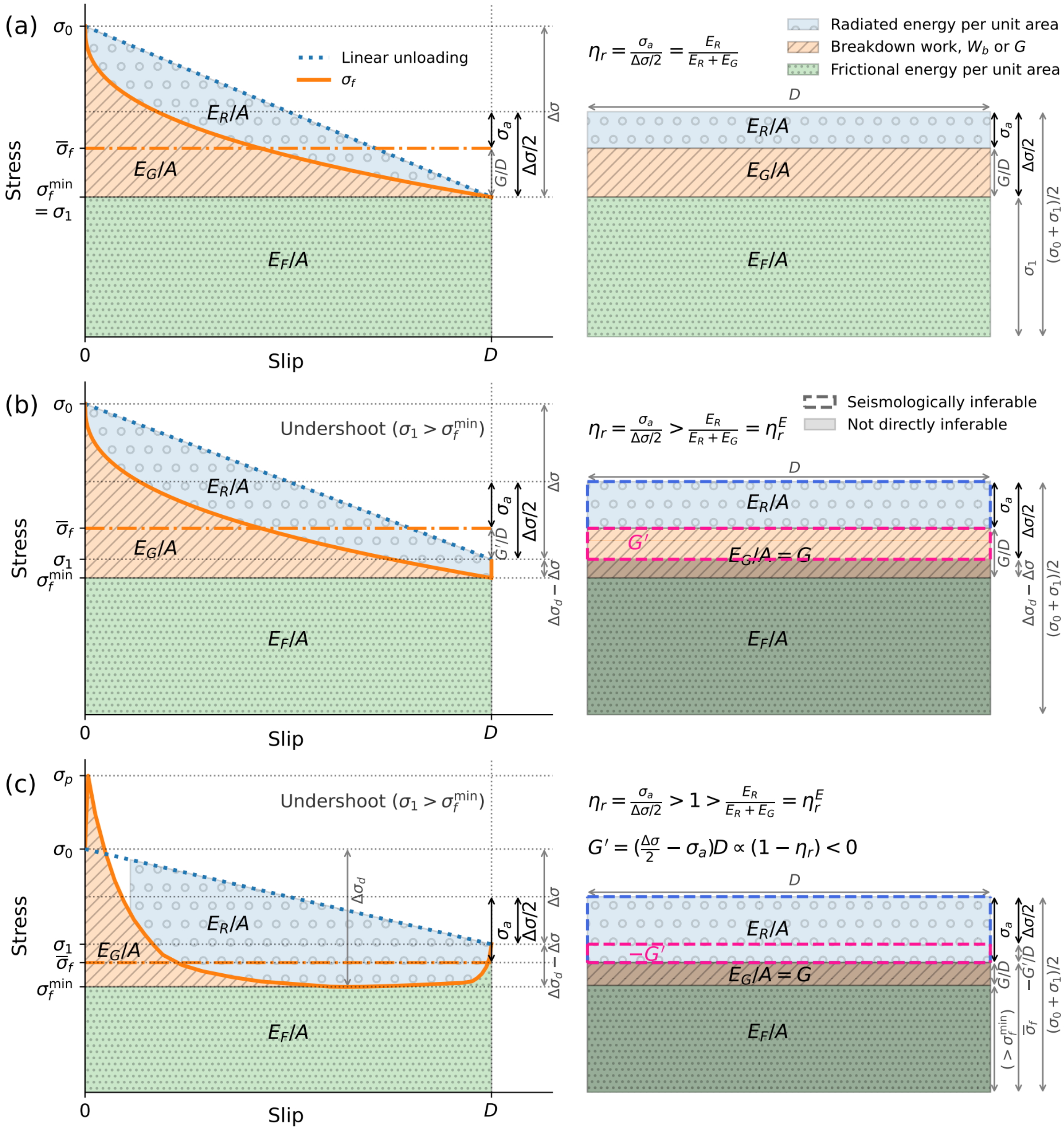

Figure 2. Schematic energy partitioning during fault slip on a unit area: (a) Case without undershoot or overshoot, where the seismological radiation efficiency $\eta_r = \sigma_a/(\Delta\sigma/2)$ directly represents the partitioning of released energy between seismic radiation and fracture processes; (b) Undershoot case where η_r reflects only part of the fracture process, so the seismologically inferred fracture energy per unit area G' is smaller than the true fracture energy G; (c) Undershoot

case where $\eta_r > 1$ and G' becomes negative. The first column is adapted from Abercrombie and Rice (2005), Cocco et al. (2023), and Lambert and Lapusta (2023); the second column recasts the same budgets in a geometric form.

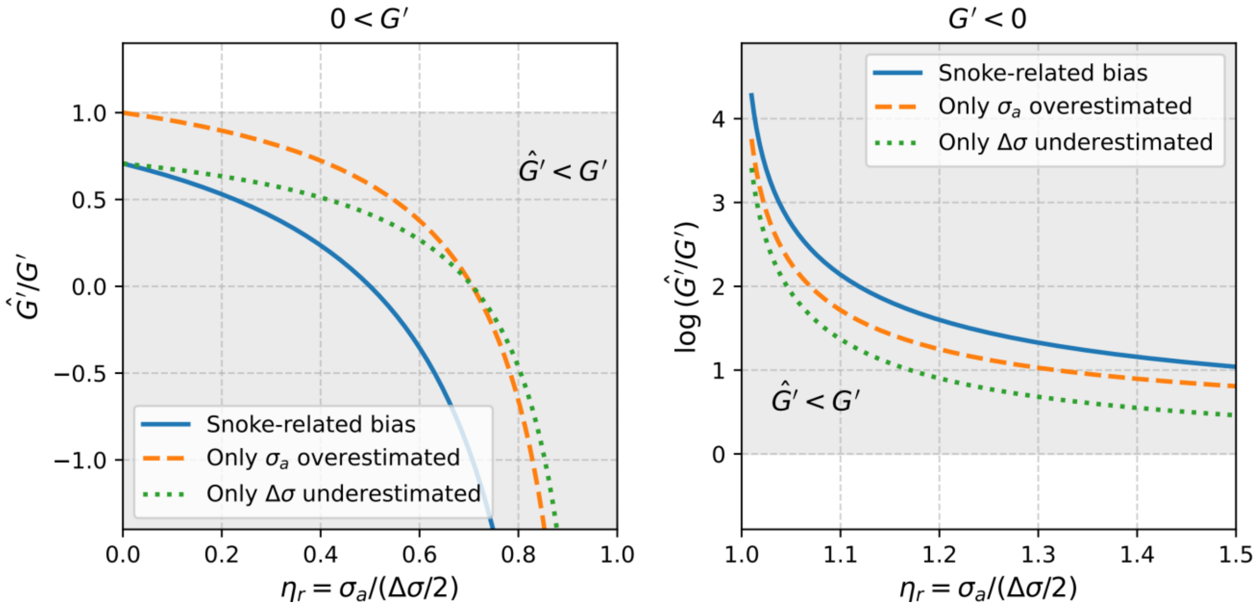

Figure 3. Relative change in inferred fracture energy per unit G' as a function of radiation efficiency or ratio η_r, illustrating how biases in the static stress drop $\Delta\sigma$ and apparent stress σ_a, arising from an underestimated low-frequency spectral level by a factor of $\sqrt{2}$, as in the Snoke formulation, affect G'. Here $\hat{G}'$ denotes the value inferred from the biased source parameters. The solid line corresponds to the case in which $\Delta\sigma$ is underestimated by $\sqrt{2}$ and σ_a is overestimated by $\sqrt{2}$. The dashed line shows the case where only σ_a is overestimated, and the dotted line shows the case where only $\Delta\sigma$ is underestimated.

APPENDIX

Clarifying Snoke's approximation of the Squared Spectral Integrals

Snoke (1987) approximated J over a limited frequency band, implicitly assuming $f_c \in (f_1, f_2)$ as

$$J_{Snoke} = \frac{2}{3}[\omega_1 \Omega_0]^2 f_1 + 2\int_{f_1}^{f_2} |\omega U(\omega)|^2 df + 2|\omega_2 U(\omega_2)|^2 f_2. \qquad \text{(A1)}$$

To reconstruct Equation (A1), we define a piecewise displacement spectrum $\widehat{U}(f)$ based on Snoke's stated assumptions of a constant amplitude below f_1 and an f^{-2} decay above f_2, with ζ being constant:

$$\widehat{U}(f) = \begin{cases} \Omega_0 & for\ \ f < f_1 \\ U(f) & for\ \ f_1 \le f < f_2. \\ \zeta f^{-2} & for\ \ f_2 \le f \end{cases}$$

(A2)

The spectral integral J, defined in Equation (2), then becomes

$$J \approx 2\int_0^{\infty} \left|2\pi f \widehat{U}(f)\right|^2 \, df = J_1 + J_2 + J_3, \qquad \text{(A3)}$$

with the individual components given by

$$J_1 = 2\int_0^{f_1} |2\pi f \Omega_0|^2 df = 2\int_0^{\omega_1} |\omega \Omega_0|^2 d\omega \frac{1}{2\pi} = \frac{2}{3}[\omega_1 \Omega_0]^2 f_1, \qquad \text{(A4)}$$

$$J_2 = 2\int_{f_1}^{f_2} |2\pi f U(f)|^2 df = 2\int_{f_1}^{f_2} |\omega U(\omega)|^2 df, \qquad \text{(A5)}$$

$$J_3 = 2\int_{f_2}^{\infty} |2\pi f \zeta f^{-2}|^2 df = 2(2\pi\zeta)^2 \int_{f_2}^{\infty} f^{-2} df = 2(2\pi\zeta)^2 f_2^{-1}. \qquad \text{(A6)}$$

Using $\widehat{U}(f_2) = \zeta f_2^{-2}$, we can express J_3 in terms of the boundary value:

$$J_3 = 2(2\pi f_2 \zeta f_2^{-2})^2 f_2 = 2\left|\omega_2 \widehat{U}(f_2)\right|^2 f_2. \tag{A7}$$

Assuming continuity at f_2, where $\zeta = U(f_2) f_2^2$ and thus $\widehat{U}(f_2) = U(f_2)$ gives

$$J_3 = 2|\omega_2 U(\omega_2)|^2 f_2. \tag{A8}$$

Taken together, Equations (A3) through (A8) reproduce the approximation J_{Snoke} proposed by Snoke (1987). A similar approximation was applied to the spectral integral K.

A notable feature is that Equations (A6) through (A8) show how the tail integral for $f > f_2$ can be approximated by the squared velocity spectrum at the boundary frequency f_2, scaled by f_2:

$$\int_{f_2}^{\infty} |V(\omega)|^2 \, df \approx f_2 |V(f_2)|^2. \tag{26}$$

This indicates that, in log-log space, the tail integral for an f^{-2} decay can be viewed as the area of a triangle equivalent to the rectangle defined by f_2 and $|V(f_2)|^2$, showing that the local value at the boundary encapsulates the entire tail contribution. This representation was further examined and refined by Ide and Beroza (2001).

Figure 1

Click here to access/download;Figure;fig1.pdf

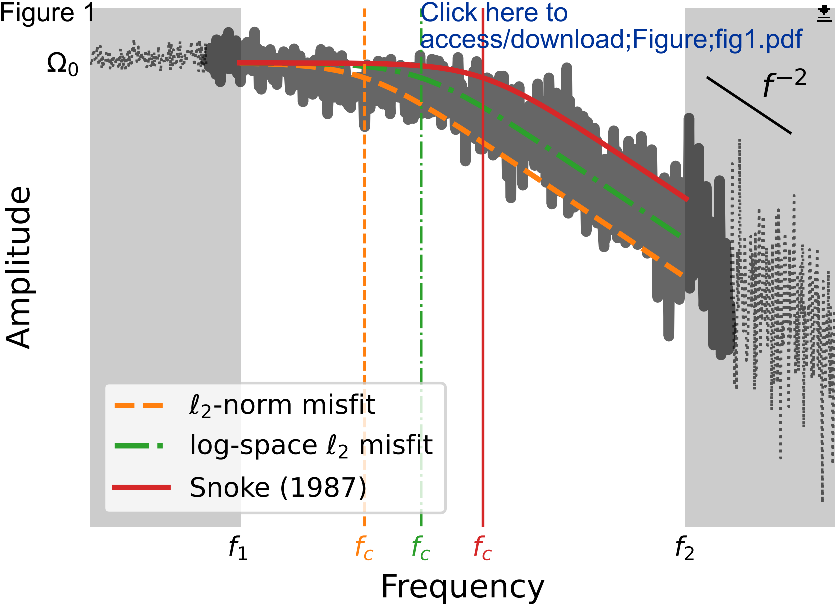

Figure 2

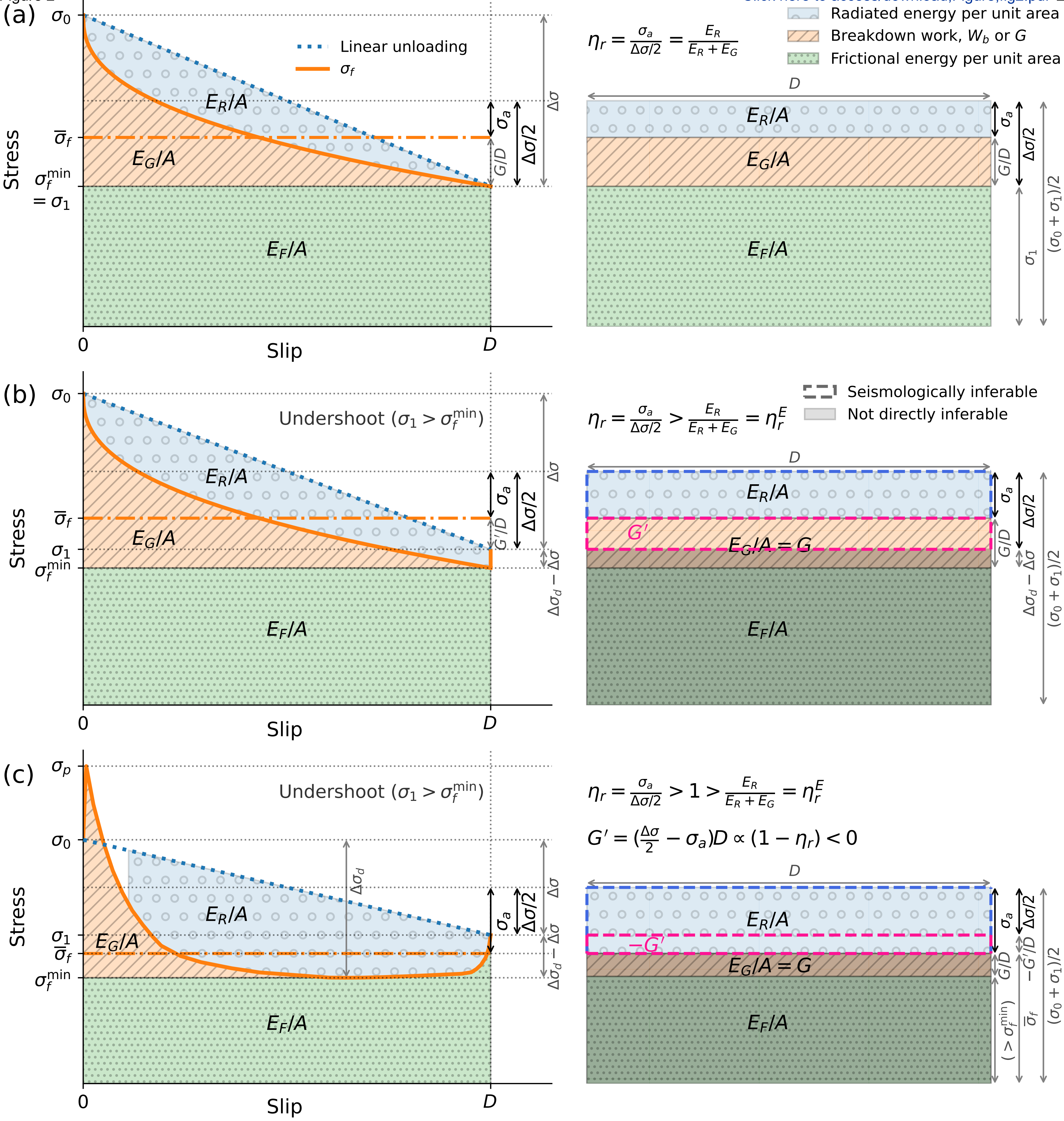

(a)
σ_0
Linear unloading
σ_f
E_R/A
$\bar{\sigma}_f$
E_G/A
$\sigma_f^{\min}$ $= \sigma_1$
E_F/A
Stress
Slip
0
D
σ_a
$\Delta\sigma/2$
$\Delta\sigma$
G/D
$\eta_r = \frac{\sigma_a}{\Delta\sigma/2} = \frac{E_R}{E_R + E_G}$
Radiated energy per unit area
Breakdown work, W_b or G
Frictional energy per unit area
σ_1
$(\sigma_0 + \sigma_1)/2$
(b)
Undershoot ($\sigma_1 > \sigma_f^{\min}$)
σ_1
G'/D
$\Delta\sigma_d - \Delta\sigma$
Seismologically inferable
Not directly inferable
$\eta_r = \frac{\sigma_a}{\Delta\sigma/2} > \frac{E_R}{E_R + E_G} = \eta_r^E$
G'
$E_G/A = G$
(c)
σ_p
$\Delta\sigma_d$
$\eta_r = \frac{\sigma_a}{\Delta\sigma/2} > 1 > \frac{E_R}{E_R + E_G} = \eta_r^E$
$G' = (\frac{\Delta\sigma}{2} - \sigma_a)D \propto (1 - \eta_r) < 0$
$-G'$
$-G'/D$
$\bar{\sigma}_f$
$(> \sigma_f^{\min})$

Figure 3

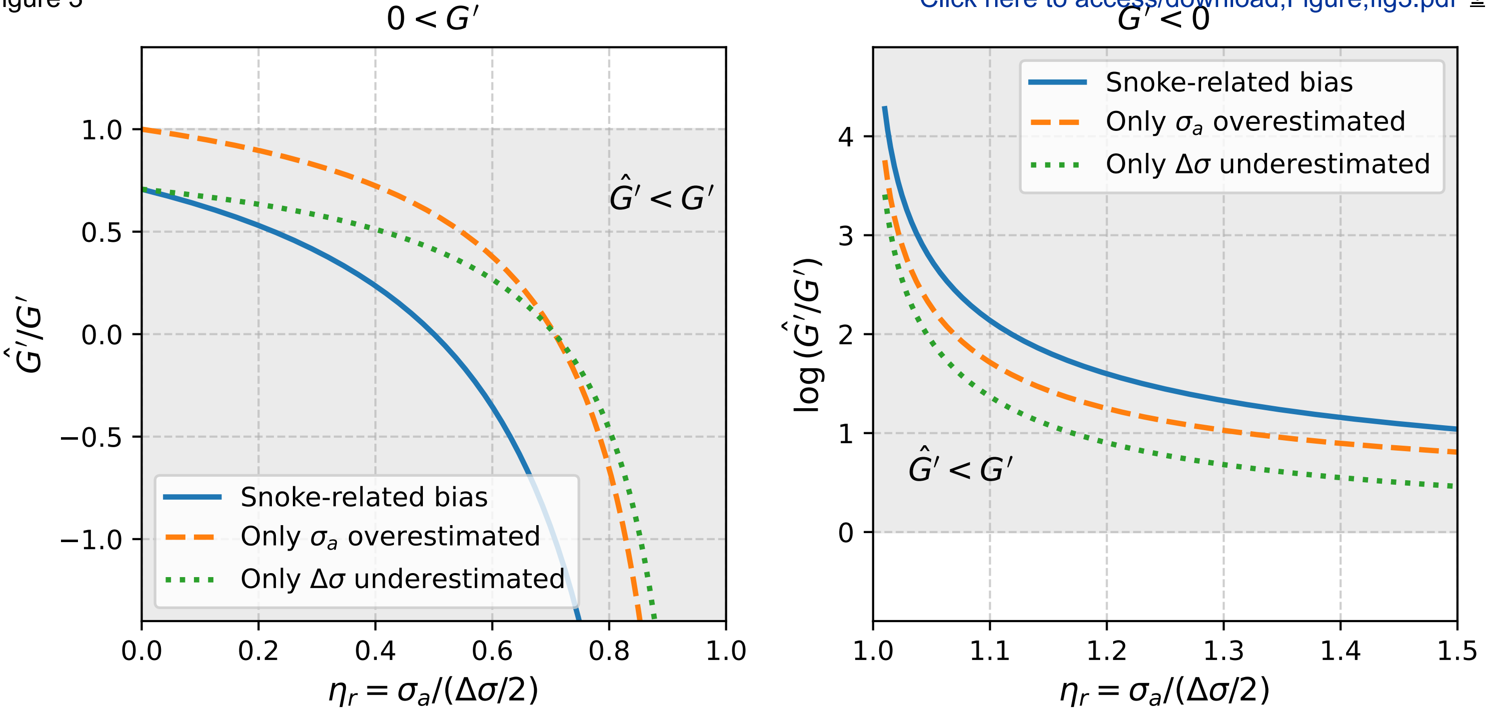
$0 < G'$
$\hat{G}' < G'$
Snoke-related bias
Only σ_a overestimated
Only $\Delta\sigma$ underestimated
$\hat{G}'/G'$
$\eta_r = \sigma_a/(\Delta\sigma/2)$
$G' < 0$
$\log(\hat{G}'/G')$
$\hat{G}' < G'$
Snoke-related bias
Only σ_a overestimated
Only $\Delta\sigma$ underestimated
$\eta_r = \sigma_a/(\Delta\sigma/2)$